Structural, magnetic, and magnetotransport properties of NiFe/Ag as-deposited multilayers for variable NiFe and Ag layer thickness

C. Christides,[a] S. Stavroyiannis, and D. Niarchos
Institute of Materials Science, NCSR ''DEMOKRITOS,'' 153 10 Agia Paraskevi, Attiki, Greece

(Received 16 April 1996; accepted for publication 11 July 1996)

Superstructure refinement analyses of x-ray-diffraction data, magnetotransport, and hysteresis loop measurements were performed in $Ni_{81}Fe_{19}$/Ag ultrathin multilayers. A ferromagnetic coupling and oscillations of coercivity H_c and residual magnetization M_r at 5 K have been observed as a function of Ag layer thickness. The observed residual stresses in NiFe layers which induce preferable magnetic easy-axes distributions along the strain direction are related with bulk spin-dependent scattering in individual layers for this type of giant magnetoresistive systems. © *1996 American Institute of Physics.* [S0021-8979(96)02320-1]

I. INTRODUCTION

In NiFe/Ag discontinuous multilayers (DML), consistent annealing is required to produce consistent grain size distributions[1,2] for optimization of the giant magnetoresistive (GMR) effect (≈5% at RT). A systematic change in the saturation magnetostriction λ_s and GMR have been observed[3] as a function of annealing temperature $T_{\rm an}$. The increase of λ_s from negative to positive values as a function of $T_{\rm an}$ suggests that the films are under tensile stress in the as-deposited state. This stress is gradually reversed with annealing and for $\lambda_s \approx 0$ the GMR is maximum. It is believed that the relieved intralayer strain effects accompanied by grain-boundary separation in NiFe layers, after annealing at 340 °C, give rise to micromagnetic changes that favor an increased interlayer antiferromagnetic (AF) exchange coupling $J_{\rm AF}$.

The observed oscillations in GMR of $Ni_{81}Fe_{19}$/Cu (Ref. 4) and Co/Cu (Ref. 5) multilayers as a function of Cu spacer thickness, measured at 4.2 and 300 K, provide evidence for the dependence of $J_{\rm AF}$ from the saturation magnetization M_s in magnetic layers. In both cases at 4.2 K well-defined oscillations in GMR are found for increasing Cu thickness. For the Co/Cu system similar oscillations are found at all temperatures from below 4.2 K to above 400 K whereas in NiFe/Cu only a single oscillation is observed at RT for magnetron sputtered multilayers. This might be a consequence of the AF coupling since in the former system $J_{\rm AF}$ at the first oscillation peak weakens by only 25% between 4.2 and 300 K, whereas in the latter $J_{\rm AF}$ changes by a factor of 2.5. Since $J_{\rm AF}$ is related to M_s, the saturation field H_s, and thickness t_F of the magnetic layers as[6] $J_{\rm AF} \approx -H_s M_s t_F/4$, it is reasonable to argue that in NiFe/Cu multilayers at low temperatures, where the AF coupling is considerably stronger, it is likely that more oscillations in coupling will be observed than at higher temperatures where the coupling may be weak compared to direct FM coupling via defects. As-deposited NiFe/Au multilayers[7] exhibit oscillatory variations in saturation MR as a function of $t_{\rm Au}$ at RT and present the largest magnetic field sensitivities yet reported. However, the estimated $J_{\rm AF}$ is much weaker than in similarly prepared NiFe/Cu and NiFe/Ag multilayers. Consequently, for this category of NiFe/NM (NM=Cu, Ag, Au) multilayers the importance of $J_{\rm AF}$ in the GMR effect has to be reconsidered.

In the present study, $Ni_{81}Fe_{19}$/Ag multilayers are examined with x-ray-diffraction (XRD) data analysis at high angles, MR measurements at RT and 5 K, and magnetic hysteresis loops measurements at 5 K for the as-deposited samples. Although a significant change of the MR effect has been observed at 5 K AF layer coupling at any temperature was not observed.

II. PRELIMINARY DETAILS

A. Experimental details

Metallic disks of $Ni_{81}Fe_{19}$ stoichiometric alloy and Ag, with diameter 5 cm and 99.99% pure, were used as target materials for magnetron sputtering deposition. Multilayers of Ag(40 Å)/[NiFe(t)/Ag($t_{\rm Ag}$)]$_{20}$—with nominal thickness t_f =15,20,25,30 Å and $t_{\rm Ag}$=10–50 Å with step 10 Å—were deposited on a p-type Si(100) substrate, 300 μm thick, at ~40 °C in a chamber with base pressure of 6×10^{-7} Torr under an Ar (99.999% pure) pressure of 3 mTorr. The substrates were cut before deposition in dimensions of 12×4 mm^2. A rf magnetron gun operating at 30 W with a deposition rate of 1 Å/s for NiFe and dc sputtering at 10 W resulting in 2.2 Å/s of Ag was used. XRD spectra were collected with a SIEMENS D500 powder diffractometer using Cu $K\alpha$ radiation at ambient temperature. MR measurements were performed with the four-point-probe method, using a dc current of 50 mA. Magnetic hysteresis loops were measured with a Quantum Design MPMSR2 superconducting quantum interference device (SQUID) magnetometer. These measurements were performed in the desired temperature by applying first the maximum positive field H parallel to film plane and then finishing the loop. Afterward the sample was taken out of the SQUID (RT) to mount it in the vertical position on the probe for the perpendicular to film field direction and then it was zero field cooled to start the measurement from the highest field first.

B. XRD analysis

The observed spectra were fitted by using the superlattice refinement (SUPREX) program developed[8,9] to allow a

[a]Electronic mail: christos@cyclades.nrcps.ariadne-t.gr

 0021-8979/96/80(8)/4512/7/$10.00

quantitative comparison between the model calculations and the measured profiles. Since our low-angle ($2\vartheta<7°$) observed profiles are not reliable for quantitative analysis only the high-angle satellite (HAS) peaks are used. For convenience, the HAS peak positions are usually indexed about the average lattice constant d:

$$\frac{2\sin\vartheta}{\lambda_x}=\frac{1}{d}\pm\frac{n}{\Lambda}, \tag{1}$$

where n is an integer that labels the order of the satellite around the main Bragg peak, λ_x is the wavelength of x rays, $\Lambda=t_f+t_{\mathrm{Ag}}+t_i$ (t_i is the interface thickness), and $d=\Lambda/(N_{\mathrm{A}}+N_{\mathrm{B}})$, with N_{A} and N_{B} the number of atomic planes of material A and B in one bilayer. From the peak positions d and Λ can be determined directly. The model uses a general kinematical one-dimensional diffraction formula, which includes random continuous and discrete fluctuations from the average structure and for which only the structure factor of one single layer of each material has to be averaged. A nonlinear fitting algorithm is used to fit the entire XRD profile, i.e., peak positions, relative intensities, and the line profiles.[9] The crystalline layer is described by N atomic planes which are separated by a lattice constant d. The distribution of the number of planes N_j and d is given by a discrete distribution about the mean values with widths σ. For every layer three atomic planes near the interface are allowed to expand or contract an amount $\Delta d_1 e^{-n\alpha}$ and $\Delta d_2 e^{-n\alpha}$ on the bottom and top, respectively, where $n=0,1,2$ corresponds to atomic planes away from the interface. The parameter α is a constant that determines the decay of the strain away from the interface and is typically assumed to be 0.55. For a lattice-mismatched incoherent interface, the interface distance δ (structural roughness) varies in a continuous manner, described with a Gaussian distribution about an average value, and the interface fluctuation (disorder) is the width c of the Gaussian. These interface-related parameters account for the estimation of t_i. Two pure Lorentz functions with identical height, mean, and width were convoluted to account for the limited instrumental resolution in the line shapes of Bragg peaks. A constant background intensity $I_b=1$ and a chi-square fitting with weighting factor 0.5 were used for the calculation of the direct XRD pattern.

III. EXPERIMENTAL RESULTS

A. XRD results

The variation of the higher-angle diffraction patterns in the vicinity of ⟨111⟩ and ⟨222⟩ Ag superlattice peaks is displayed in Figs. 1 and 2 for $t_f\approx 20$ Å as a function of t_{Ag} and for $t_{\mathrm{Ag}}\approx 40$ Å versus t_f, respectively. The solid line is the calculated profile from SUPREX refinement and the obtained parameters are listed in Table I. The observed spectra display two important features, as follows.

First, the intensity I_n of the $n=0$ Bragg peak I_0 is insensitive for the samples with $t_f\approx 20$ Å as a function of Ag thickness while for those with fixed $t_{\mathrm{Ag}}\approx 40$ Å I_0 tends to zero as t_f increases from 16 to 25 Å and I_{-2} becomes stronger at the same time. For $t_{\mathrm{Ag}}=40$ Å and $t_f=30$ Å, I_0 almost disappears while the I_{-1} and I_{-2} components become very

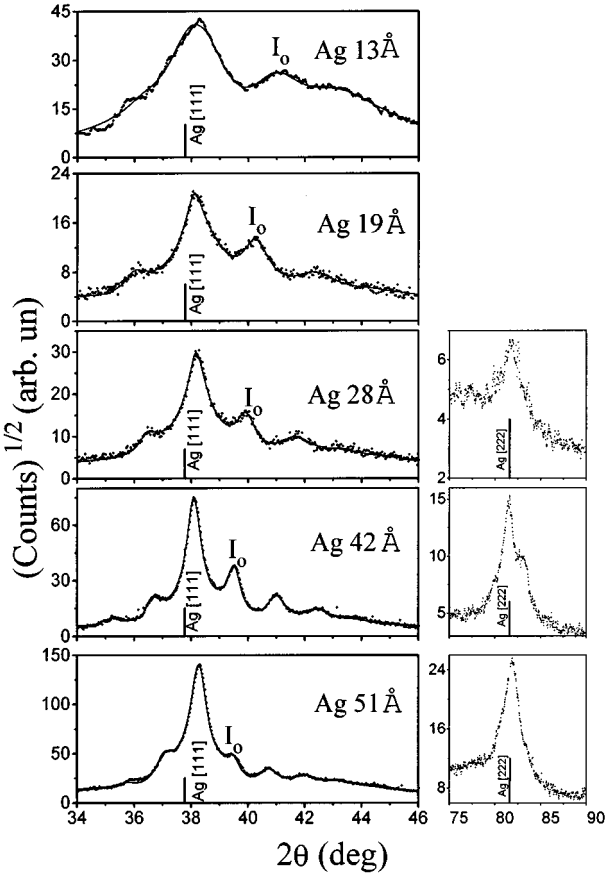

FIG. 1. XRD profiles for different Ag layer thickness. The solid line is a fit from SUPREX. The position of the zeroth-order satellite peak is marked with I_0. The displayed t_{Ag} values are taken from Table I.

intensive. It is known that interface roughness effects, such as layer thickness fluctuations and interfacial diffusion, can cause damping, broadening, and shifting of the $n\neq 0$ satellite peaks but they cannot reduce the $n=0$ peak to be less intensive from the satellites. Therefore, stress effects are responsible for the damping of I_0 peak.

Second, in Ag ⟨222⟩ peak position there is a double Bragg reflection for $t_f=16$ Å which merges to a single peak as the NiFe layer becomes thicker for constant $t_{\mathrm{Ag}}\approx 40$ Å. For $t_f\approx 20$ Å as a function of t_{Ag}, the Ag ⟨222⟩ peak is lost in the background for $t_{\mathrm{Ag}}=13$ and 19 Å while only for $t_{\mathrm{Ag}}=42$ Å is an additional reflection clearly seen. Note that the diffraction pattern for $t_{\mathrm{Ag}}=42$ Å and $t_f=18$ Å appears in both Figs. 1 and 2 for a better comparison. Consequently, residual stresses and nucleation of Ag grains through NiFe grain-boundary diffusion[4,5] might be related to the observed variations of the spectra.

The estimated values from SUPREX for the lattice expansion of the atomic planes of NiFe and Ag near the interface are plotted in Fig. 3. The zero layer in Fig. 3 corresponds to the bilateral plane that separates the first atomic layer of each component at the interface. The displayed lattice relaxation is calculated by adding to d_f or d_{Ag} values in Table I the corresponding $\Delta d_1 e^{-n\alpha}$ (open symbol) and $\Delta d_2 e^{-n\alpha}$ (solid symbol) parameters for every layer ($n=0,1,2$). The four-layer in Fig. 3 corresponds to d_f or d_{Ag} values from Table I.

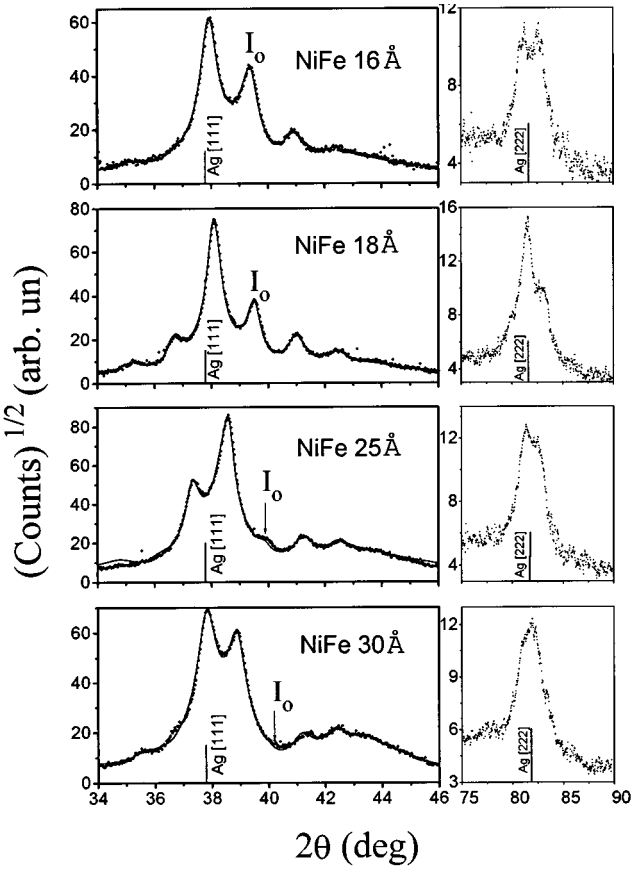

FIG. 2. XRD profiles for different NiFe layer thickness. The position of the zeroth-order satellite peak is marked with I_0. The solid line is a fit from SUPREX. The displayed t_f values are taken from Table I.

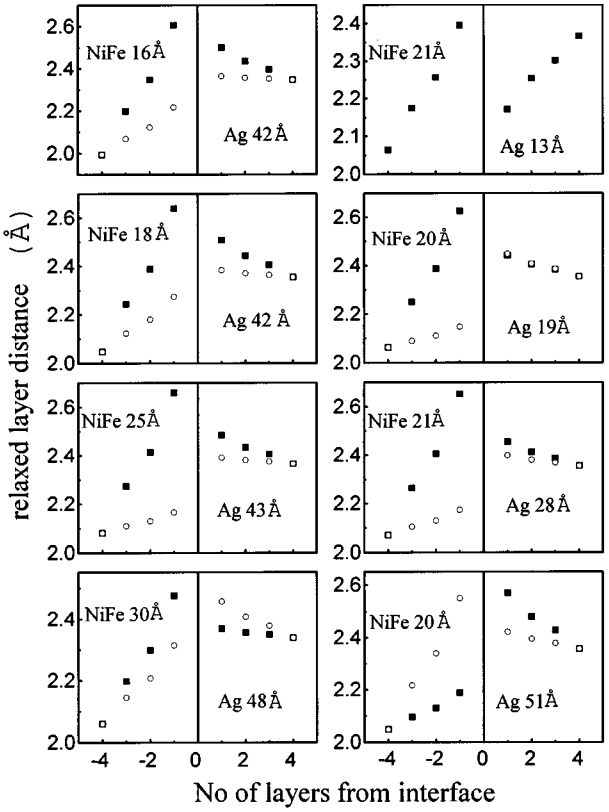

FIG. 3. Estimated values from SUPREX for the lattice expansion of the atomic planes of NiFe and Ag near the interface.

Only for the sample with NiFe(21 Å)/Ag(13 Å), where $N_{\mathrm{Ag}}<7$, it is assumed: $\Delta d_1=\Delta d_2$ for every layer, because there is a direct correlation with d_f or d_{Ag} that gives large uncertainties in the final results. For this sample the roughness parameter δ is close to the $(d_f+d_{\mathrm{Ag}})/2$ value.

In Fig. 3 there are two major results, as follows:

(i) The expansion of the NiFe layer is always considerably large (~0.4 Å) compared to the moderate relaxation of Ag (~0.1 Å) except for $t_f=21$ Å and $t_{\mathrm{Ag}}=13$ Å where d_{Ag} seems to contract at the interface due to the imposed constrain $\Delta d_1=\Delta d_2$ described above. The large NiFe interface expansion may arise from both strain effects and varied alloy composition. For γ-(Ni,Fe) phases (JCPDS, No. 23-297) the lattice constant varies from 3.5956 Å ($d_{111}=2.076$ Å for 39 at. % Ni) to 3.5238 Å ($d_{111}=2.034$ Å for Ni 100%). These values are considerably smaller to those obtained and therefore strain effects are eminent at interfaces.

(ii) For thinner NiFe (<25 Å) and Ag (<45 Å) layers the expansion on the top of every layer (dark symbol) is more pronounced relative to bottom which imply that the multilayer film has a concave bending relative to Si substrate. Since a lattice expansion is apparent in both the top and bottom of the NiFe and Ag layers, their presence can be explained by misfit dislocations and/or atomic intermixing of NiFe with Ag atoms. The fact that the refined roughness parameter δ is always less than the average $(d_f+d_{\mathrm{Ag}})/2$ value (see Table I) is an indication that chemical interdiffusion occurs. However, NiFe and Ag are immiscible and, hence, the interdiffusion can be considered here as a penetration of atoms into grain boundaries at the interface.

TABLE I. Refined parameters from SUPREX. The parameters are explained in the text.

Sample	d_f (Å)	d_{Ag} (Å)	N_f (Å)	N_{Ag} (Å)	t_f (Å)	t_{Ag} (Å)	δ (Å)	c (Å)	Λ (Å)	$\sigma(N_f)$	$\sigma(N_{\mathrm{Ag}})$
NiFe(20 Å)/Ag(10 Å)	2.064	2.367	11.054	6.675	21.385	13.06	2.26	0.50	38.97	0.12	2
NiFe(20 Å)/Ag(20 Å)	2.060	2.355	10.21	8.82	20.22	18.77	1.79	0.31	42.57	0.13	2.43
NiFe(20 Å)/Ag(30 Å)	2.070	2.355	10.68	12.65	21.35	27.70	1.78	0.30	52.62	0.26	2.70
NiFe(20 Å)/Ag(40 Å)	2.048	2.354	9.05	18.69	18.04	41.99	1.59	0.26	63.21	0.31	2.36
NiFe(20 Å)/Ag(50 Å)	2.049	2.357	10	22.33	19.66	50.81	1.65	0.28	73.77	0.91	2.95
NiFe(15 Å)/Ag(40 Å)	1.994	2.346	8.17	18.76	15.90	41.98	1.84	0.28	61.57	0.32	2.91
NiFe(25 Å)/Ag(40 Å)	2.081	2.366	12.25	19.01	24.68	42.89	1.48	0.07	70.53	1.37	3.10
NiFe(30 Å)/Ag(40 Å)	2.060	2.399	14.97	21.52	30.05	48.28	1.90	0.39	82.14	0.50	2.2

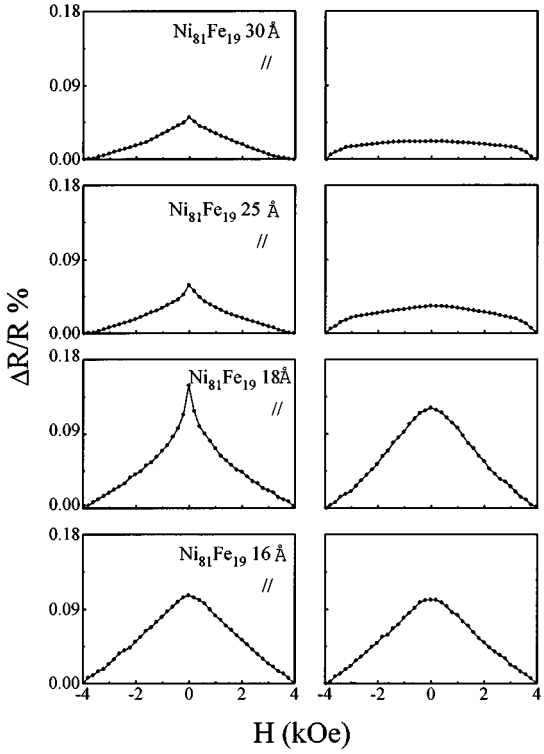

FIG. 4. MR measurements at RT for NiFe(t_f)/Ag(40 Å) as-deposited films, with the external magnetic-field direction parallel (right-hand side) and perpendicular (left-hand side) to film plane.

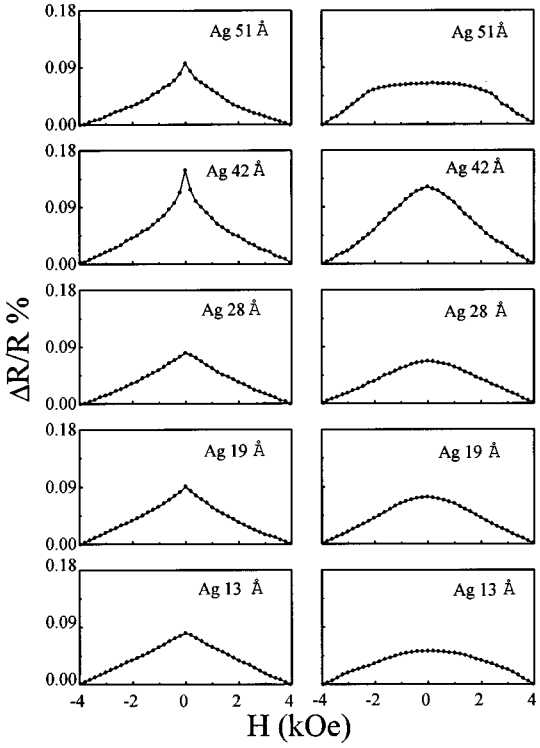

FIG. 5. MR measurements at RT for NiFe(20 Å)/Ag(t_{Ag}) as-deposited films, with the external magnetic-field direction parallel (right-hand side) and perpendicular (left-hand side) to film plane.

For thicker layers the strain effects, in NiFe(30 Å)/Ag(48 Å), are likely to equilibrate since the expansion of the bottom Ag layer exceeds that on top and vice versa for the NiFe layer. This results to a better matching of NiFe/Ag layers (see left-hand bottom in Fig. 3) by creating tensile and compressive interlayer strain in NiFe and Ag layers, respectively. The change in intensities of the superstructure pattern (Fig. 2 bottom) clearly shows the difference. A possible interpretation of changes in elastic strain with increasing thickness is the approach[10] to critical thickness t_c, that d_f and d_{Ag} relax to its bulk crystal spacing. As seen in Table I the relaxed d_f and d_{Ag} values are close to bulk values 2.048 and 2.359 Å, respectively, only for the NiFe(20 Å)/Ag(40 Å) sample. An alternative explanation fit better with the study of microstructure and magnetoelastic (ME) coupling coefficients in ultrathin $Ni_{80}Fe_{20}$/Ag films by Song, Kim, and O'Handley.[11] It is observed that the effective ME coefficients B^{eff} of polycrystalline films have a surface dependent component which varies inversely with film thickness t_f. This component can change the sign of B^{eff} and dramatically increase its magnitude for $t_f \leqslant 26$ Å, while it is close to zero for $t_f \approx 30$ Å.

In NiFe(20 Å)/Ag(51 Å), while there is a more pronounced expansion of bottom NiFe layer that matches the expansion of top Ag, a mismatch of top NiFe and bottom Ag appears. Since interfacial roughness is still experimentally difficult to distinguish from interfacial diffuseness, the present data are not sufficient to provide a complete explanation of interface structural modulation.

B. MR results

In Figs. 4 and 5 are shown MR measurements at RT for NiFe(t_f)/Ag(40 Å) and NiFe (20 Å)/Ag (t_{Ag}) as deposited films, respectively, with the external magnetic-field direction parallel (right-hand side) and perpendicular (left-hand side) to film plane. It is observed (Fig. 4) that the MR effect is isotropic for $t_f = 16$ Å while the maximum MR is achieved for NiFe(18 Å)/Ag(42 Å), which shows a characteristic sharpening of the curve around zero field in the parallel direction. There is only one maximum of $\Delta R/R$ at zero field and the rounding of the curve for the perpendicular field direction is caused from film shape anisotropy.

MR measurements were performed at 5 K and the observed curves are shown in Fig. 6 for some selected samples. A considerable change in the response of transport properties to magnetic field variation occurs relative to RT measurements. For NiFe(18 Å)/Ag(42 Å) the effect is almost isotropic. Two common features appear in these measurements:

(i) Saturation of the MR effect is not achieved and there is a linear decrease with increasing field above 0.5 T (the linear variation might be attributed to superparamagnetic NiFe particles);
(ii) two maximum values of $\Delta R/R$ exist for nonzero negative and positive fields.

Note that the maximum MR effect, of 1.5% at RT for $H_s = 100$ Oe, has been observed for NiFe(20 Å)/Ag(40 Å) after 3 h annealing at 400 °C, in a vacuum-sealed Pyrex tube. In all annealed samples a coercive field H_c was apparent in the maxima of $\Delta R/R$ loops.

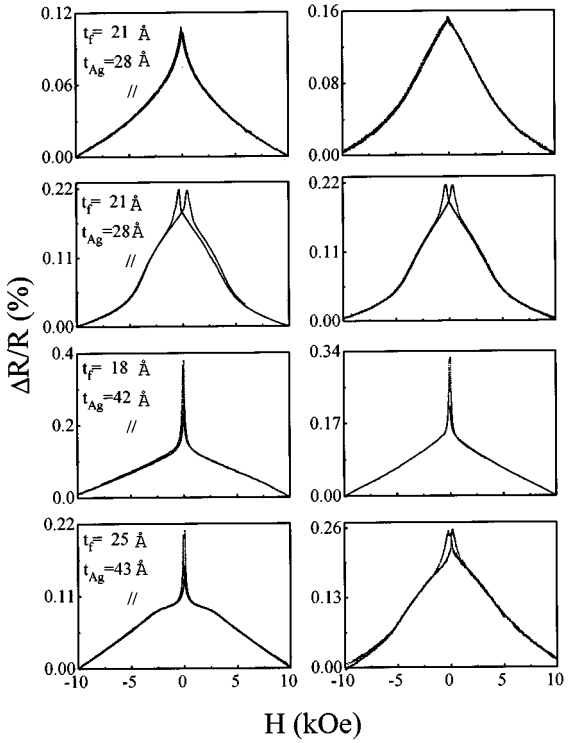

FIG. 6. MR measurements at 5 K for selected NiFe/Ag as-deposited films, with the external magnetic-field direction parallel (right-hand side) and perpendicular (left-hand side) to film plane.

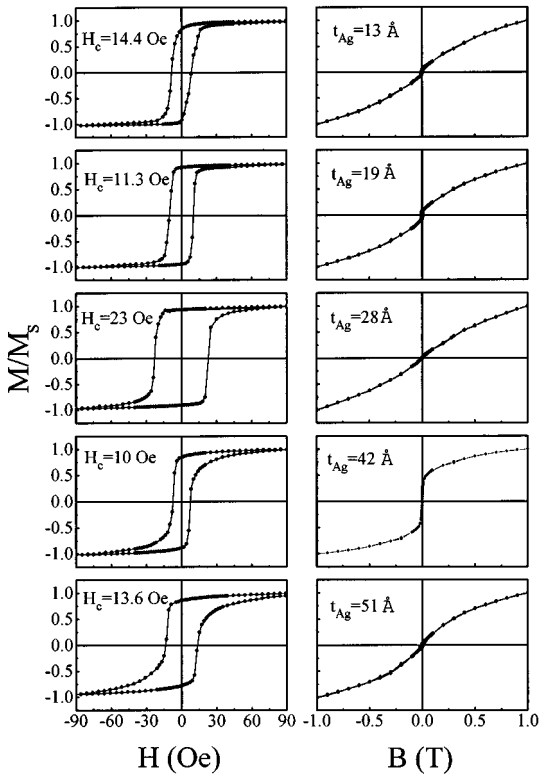

FIG. 7. Hysteresis loops measured at 5 K for NiFe(20 Å)/Ag(t_{Ag}) as-deposited films, with the external magnetic-field direction parallel (right-hand side) and perpendicular (left-hand side) to film plane.

C. Magnetic hysteresis

Isothermal SQUID magnetic measurements were performed with the field applied parallel ($H_{\parallel}$) and perpendicular ($H_{\perp}$) to the film plane at 300, 100, and 5 K. The loop shape was characteristic of ferromagnetically (FM) coupled material without any detectable coercive field H_c above 100 K. Figures 7 and 8 display the observed loops at 5 K where a significant H_c has been observed. It is worth noting that for a pure $Ni_{81}Fe_{19}$ (1000-Å-thick) film on Si(100), no coercivity more than ~1 Oe was observed at any temperature. A comparison of loops, with $H_{\parallel}$, for samples with variable t_{Ag} (Fig. 7, left-hand side) to those with variable t_f (Fig. 8, left-hand side) shows that H_c remains higher than 10 Oe and oscillates as a function of t_{Ag} (Fig. 9) while a decrease from 24.4 Oe to a bottom value of ≈4 Oe is observed for increasing t_f. For $H_{\perp}$ the loop shape is similar to that expected for uniaxial particles with their easy axes (EA) randomly oriented[12] with an exception for NiFe(20 Å)/Ag(40 Å) and NiFe(25 Å)/Ag(40 Å), where rotation of magnetic moments out of film plane is ''easier'' and the shape anisotropy does not modify the loop like in the other samples. For both samples, with $H_{\perp}$ geometry, $H_c \approx 16$ Oe is obtained with a reduced remanence $M_r/M_s = 0.18$ and 0.03 for $t_f = 20$ and 25 Å, respectively. The variation of d_f from Table I, H_c, and M_r/M_s as a function of t_{Ag} and t_f at 5 K is presented in Fig. 9. The resemblance of d_f and H_c oscillations is seen as a function of t_{Ag} but not for variable t_f. The dependence of d_f and H_c with t_f in Fig. 9 indicates that there is not a direct relationship between them caused from variable strain. Here, for d_f larger than the relaxed 2.048 Å value H_c approaches a low limit as a function of t_f probably due to proportionality of H_c with the anisotropy field $H_A (= \alpha K/M_s$, α is the grain shape and domain-dependent constant) in a first approximation. The reported[13] variation of M_s with t_f (for $t_f < 50$ Å) may explain the observed H_c vs t_f dependence. Since our XRD analysis exclude the possibility of ''bridging'' among NiFe layers through Ag, that might vary H_c as well, variations in H_c and d_f with t_{Ag} can be understood in terms of stress-induced anisotropy in ultrathin magnetic films.

For thin films it is realized, with qualitative reasoning, how stress-induced reorientation of magnetization on the hysteresis loop parameters infers reduction or increase of M_r and H_c.[14] In this case it is assumed that the initial films are roughly isotropic; this means that the local anisotropy, which determines the domain structure (crystalline and local stress anisotropy), has an isotropic distribution of the local intrinsic EA for an assembly of noninteracting domains. Accordingly, it is shown[15] that in Ni films the effect of stress on the coercive force can be understood by considering two different micromagnetic reversal processes: irreversible rotation and domain-wall motion. Using these two mechanisms for magnetization reversal and the influence of the magnitude of the antiferromagnetic coupling the shapes of MR curves in both cases have been calculated for Fe/Cr films as well.[6]

In our samples we have shown that the variation of t_{Ag} creates different residual stresses. Therefore, the reorientation of magnetization can be modified in a similar manner with the externally applied stress case. The key point is that stress gives rise to the appearance of an EA in a nearly oth-

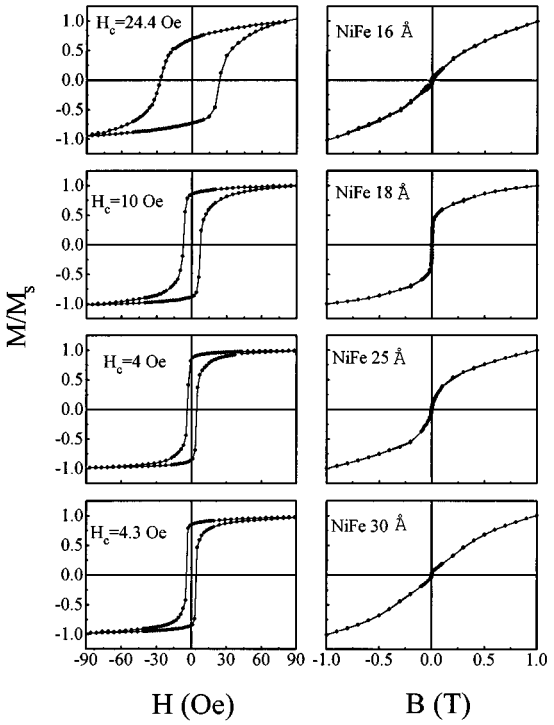

FIG. 8. Hysteresis loops measured at 5 K for NiFe(t_f)/Ag(40 Å) as-deposited films, with the external magnetic field direction parallel (right-hand side) and perpendicular (left-hand side) to film plane.

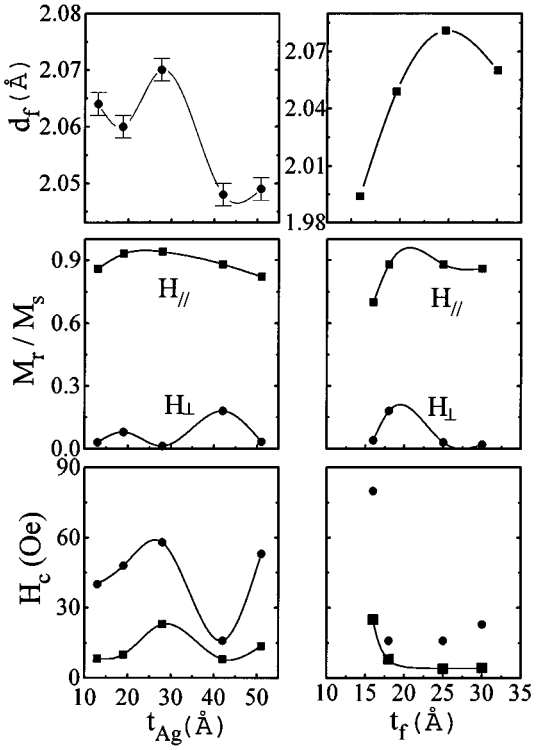

FIG. 9. Variation of the estimated d_f from Table I (top), observed M_r/M_s (middle), and H_c (bottom) values as a function of t_{Ag} (left-hand side) and t_f (right-hand side) at 5 K. Solid lines are guides to the eye. Squares are for $H_{\|}$ and circles for $H_{\perp}$ directions.

erwise isotropic film. It is shown in Ni films[15] that an EA induced by stress is consistent with the relative value of the anisotropy energies involved. If the order of magnitude of the crystalline anisotropy energy K_u is comparable to the stress-induced anisotropy K_s it is expected that the second will produce noticable effects. The residual stress may cause additional negative or positive magnetostriction λ_s even in $Ni_{81}Fe_{19}$,[13] which induces a preferable EA in every layer. By this action, for a material having a homogeneously positive magnetostriction, as in γ-(Ni, Fe), the originally isotropic distribution of domain orientations will be squeezed into a narrower distribution along an EA parallel or vertical to the film plane if the induced strain is tensile or compressive, respectively. The observed loops in Fig. 8 are indicative that the EA lies in the film plane but for NiFe(20 Å)/Ag(40 Å) and NiFe(25 Å)/Ag(40 Å), where magnetization reversal is easier for $H_{\perp}$, it may be implied that K_s is minimal and the isotropic distribution of domain orientations is maintained. From Fig. 6 it is seen that only for these two samples is there an abrupt low-field GMR effect, obviously related to easy magnetization reversal.

IV. DISCUSSION AND CONCLUSIONS

This work presents for first time a systematic variation of MR-related properties as a function of Ag and NiFe layer thickness in as-deposited thin films. The major concern is to investigate the mechanisms that primarily affect the GMR in this class of DML films. The spin-dependent scattering (SDS) obviously derives from the magnetic layers, but of particular importance is whether this SDS occurs within the interior of the magnetic layers (bulk scattering) or predominantly at the interfaces between the magnetic and spacer layers (interfacial scattering).

The interfacial scattering was examined by inserting a third material (Co) at the interfaces of NiFe/Cu films[16] and the MR effect has been dramatically enhanced at RT and 5 K. This has been attributed primarily to reestablishment of AF coupling at RT,[15] but it was attributed ultimately interfacial scattering at 5 K. Further analysis of these results[17] in terms of mean free paths for bulk SDS and interface SDS transmission coefficients indicates that SDS in FM/Cu is mainly bulk in NiFe, a mixture of bulk and interfacial in Co/Cu, and mainly interfacial in Fe/Cu.

Our analysis of NiFe/Ag as-deposited ultrathin films from XRD data shows that there is significant interface strain which is modified as a function of layer thickness. The observed splitting of $\langle 222\rangle$ Ag superlattice peak for $t_f<25$ Å is assigned to Ag interdiffusion between NiFe grain boundaries. The MR and hysteresis loop data show that for $t_f\approx 18$–25 Å and $t_{\mathrm{Ag}}\approx 38$–$43$ Å the film is magnetically isotropic and present easy magnetization reversal for low applied fields. The oscillatory variation of H_c and M_r/M_s as a function of t_{Ag} can be explained in terms of preferable EA directions in every NiFe layer induced from residual magnetostriction. The hysteresis loop shapes are typical of FM coupled layers and exhibit a nonzero coercive field below 100 K. The increase of GMR effect and $\Delta R/R$ field sensitivity at 5 K show that an enhancement of the average magnetic moment and hardening of magnetization reversal in individual NiFe layers (bulk-scattering model) have a major

contribution. In conclusion, an isotropic EA distribution of magnetic domains—due to small residual intralayer strain effects—favors of low-field GMR in sputtered NiFe/Ag multilayers.

ACKNOWLEDGMENTS

This work has been supported from the EKBAN-280 project of the General Secretariat for Research and Technology of the Development Ministry in Greece. The SUPREX refinement program was developed with funds provided by the U.S. Department of Energy and the Belgian Interuniversity Attraction Pole Program.

[1] T. L. H. Hylton, K. R. Coffey, M. A. Parker, and J. K. Howard, Science **261**, 1021 (1993).
[2] M. A. Parker, T. L. Hylton, K. R. Coffey, and J. K. Howard, J. Appl. Phys. **75**, 6382 (1994).
[3] Y. K. Kim and S. C. Sanders, Appl. Phys. Lett. **66**, 1009 (1995).
[4] S. S. P. Parkin, R. Bhadra, and K. P. Roche, Phys. Rev. Lett. **66**, 2152 (1991).
[5] S. S. P. Parkin, Appl. Phys. Lett. **60**, 512 (1992).
[6] W. Folkerts, J. Magn. Magn. Mater. **94**, 302 (1991); W. Folkerts and S. T. Purcell, *ibid*. **111**, 306 (1992).
[7] S. S. P. Parkin and T. Rabedeau, Appl. Phys. Lett. **68**, 1162 (1996).
[8] I. K. Schuller, Phys. Rev. Lett. **44**, 1597 (1980); W. Sevenhans, M. GGijs, Y. Bruynseraede, H. Homma, and I. K. Schuller, Phys. Rev. B **34**, 5955 (1986).
[9] E. E. Fullerton, I. K. Schuller, H. Vanderstraeten, and Y. Bruynseraede, Phys. Rev. B **45**, 9292 (1992).
[10] D. W. Pashley, in *Materials Science and Technology*, edited by R. W. Cahn, P. Haasen, and E. J. Kramer (VCH, Weinheim, 1991), Vol. 15, Chap. 7, pp. 290–328.
[11] O. S. Song, C. K. Kim, and R. C. O'Handley, J. Appl. Phys. **79**, 3141 (1996); O. S. Song, C. A. Ballentine, and R. C. O'Handley, Appl. Phys. Lett. **64**, 2593 (1994).
[12] B. D. Cullity, *Introduction to Magnetic Materials* (Addison–Wesley, Reading, MA, 1972), Chap. 9.
[13] M. S. Cohen, in *Handbook of Thin Film Technology*, edited by L. I. Maissel and R. Glang (McGraw–Hill, New York, 1983), Chap. 17, pp. 24–27 and 32–39.
[14] I. J. Garshelis, J. Appl. Phys. **73**, 5629 (1993).
[15] L. Callegaro and E. Puppin, Appl. Phys. Lett. **68**, 1279 (1996); E. Puppin and L. Callegaro, IEEE Trans. Magn. **MAG-32**, 281 (1996).
[16] S. S. P. Parkin, Appl. Phys. Lett. **61**, 1358 (1992).
[17] B. Dieny, V. S. Speriosou, J. P. Nozières, B. A. Gurney, A. Vadyayev, and N. Ryzhanova, *Magnetism and Structure in Systems of Reduced Dimension*, edited by R. F. C. Farrow, B. Dieny, M. Donath, A. Fert, and B. D. Hermsmeier, NATO ASI Series B, Vol. 309 (Plenum, New York, 1993), p. 279.